EPJ Web of Conferences **188**, 04001 (2018) https://doi.org/10.1051/epjconf/201818804001
JDN 23

Neutron reflectivity for soft matter

Fabrice Cousin and Alexis Chennevière

Laboratoire Léon Brillouin, CEA-CNRS, CEA-Saclay, 91191 Gif sur Yvette, France

Abstract. Specular neutron reflectivity is a technique enabling the measurement of coherent neutron scattering length density profile perpendicular to the plane of a surface or interface, and thereby the profile of chemical composition. The characteristic sizes that are probed range from around 5Å up 5000 Å. It is a scattering technique that averages information over the entire surface and it is therefore not possible to obtain information on correlations in the plane of the interface. The specific properties of neutrons (possibility of tuning the contrast by isotopic substitution, negligible absorption, low energy of the incident neutrons) makes it particularly interesting in the fields of soft matter and biophysics. This course is composed of three parts describing respectively its principle, the experimental aspects (diffractometers, samples), and some scientific examples of neutron reflectometry focusing on the use of contrast variation to probe polymeric systems.

Résumé. La réflectivité spéculaire des neutrons est une technique permettant de mesurer le profil de densité de longueur de diffusion cohérente de neutrons, et ce faisant le profil de composition chimique, perpendiculairement à une surface ou une interface plane. Les tailles caractéristiques sondées sont de l'ordre de 5Å à 5000Å. C'est une technique de diffusion qui moyenne l'information sur l'ensemble de la surface et qui ne permet donc pas d'obtenir d'informations sur les corrélations dans le plan de l'interface. Les propriétés spécifiques des neutrons (possibilité de moduler le contraste par substitution isotopique, absorption négligeable, faible énergie des neutrons incidents) la rendent particulièrement intéressante dans les domaines de l'étude de la matière molle et de la biophysique Ce cours est composé de trois parties décrivant respectivement son principe, les aspects expérimentaux (appareils de mesure, échantillons) et quelques exemples d'expériences axés sur l'utilisation de la variation de contraste pour l'étude de systèmes polymériques.

1 Introduction

Neutron reflectivity (NR) is a technique enabling to measure the thickness and the chemical composition of one or several thin layers at a surface or at an interface. Typically, length scales in the range from 5 - 5000 Å can be probed.. The principle is to measure the coefficient of reflection R of a neutron beam sent in grazing incidence on the surface that is to be studied. In this course, we will focus only on the *specular*[*] reflectivity that provides only the profile of chemical composition *perpendicular to the surface*. This specular reflectivity corresponds to the case where the incident and reflected neutron

[*] From the Latin adjective *specularis* that stands for "pertaining to mirrors, mirror-like".

beams are symmetric with respect to the surface normal. In such geometry, NR does not provide any information on the possible in-plane structure at the surface. It is thus usually very valuable to combine NR with a technique enabling to determine such in-plane structure information, either a scattering method (Grazing Incidence Small Angle Neutron Scattering, surface diffraction, off-specular measurements) or a microcopy technique (Atomic Force Microscopy, Transmission Electron Microscopy, Brewster microscopy…).
The lower limit of thickness that can be measured is directly linked to the minimal reflectivity that can be experimentally obtained. Given the actual brightness of the neutrons sources, such minimal reflectivity is of the order of 10^{-6} to 10^{-7} on samples of a few cm^2. This is of the same order of magnitude of what can be measured by X-Ray reflectivity, whose principle is similar to NR, on laboratory instruments. Such minimal X-Ray reflectivity can be extended down to lower reflectivities on synchrotron sources due to the high brilliance of such sources. X-rays measurements have thus to be preferred in many experimental cases and are in any case very complementary to NR measurements as they provide the electron density profile.

Neutrons have, however, some unique specific properties with respect to photons that enable some measurements impossible with X-rays, such as the characterization of buried interfaces, the study of materials containing hydrogen or for magnetic materials. Such specificities have made NR experiments very popular since the early 90's:
-First, **the neutron-matter interaction directly occurs between the neutron and the nuclei of atoms**, and not with the electronic cloud, as for X-rays. It differs from one isotope of a given atom to another and varies randomly from one atom to another along the periodic table of elements. In particular, hydrogen ^1H has a very different value than the ones of all other atoms constitutive of organic molecules (C,O,N..) and, last but not least, than those of deuterium ^2H. This enables to achieve experiments on organic materials because the neutron refraction index is essentially dependent on its content on hydrogen atoms. In particular, the replacement of some hydrogen atoms of a molecule by deuterium atoms will strongly modify its refraction index without altering significantly its physical and chemical properties. This opens the way to **contrast variation experiments** where some molecules are labeled by deuterium to create a neutron contrast in the system. It is also possible to continuously tune the neutron refractive index of a solvent in a complex system by mixing hydrogenated and deuterated solvents in order to *match* the one of a component, making it invisible from the neutron point of view. Such contrast variation experiments, which have been very successfully applied in soft matter in the field of surfactants [1] and polymers [2] or in biophysics [3][4].
- Second, neutrons are **very weakly absorbed** by matter, except few atoms of periodic table that have a huge neutron absorption cross-section (boron, gadolinium, lithium, ...). The imaginary part of the neutron refractive indexes is usually negligible, and not considered in neutron reflectivity calculations, contrarily to calculations of X-Ray reflectivity. This weak interaction opens the way to the study of **buried interfaces** or to achieve ***in situ* experiments in various sample environments**.
-Third, the energy of neutrons that are used for experiments whose wavelengths lay typically in the range 1 Å – 20 Å have an energy of a few meV, contrarily to X-rays that have an energy of a few keV for the same wavelengths. **The NR experiments are thus absolutely not destructive**.
Please note that neutrons have also another very important **specificity,** namely **their ability to interact with the atoms that bear a magnetic moment because they** bear a spin ±½. This enables the measurement of the magnetization profile in thin magnetic films. This aspect is out of scope of this introduction course focused on soft matter. A very good description of the magnetic neutron reflectivity principles can be found in the following reference by Fermon *et al*[5], in particular the treatment of magnetic neutron reflectivity that necessitates a formalism more complicated than those that will be described in the following.

This course is divided in three parts. We will present in the first part the principle of NR by an approach where the spin of neutrons is not taken into account. Besides, the other aspects of *grazing incidence scattering* (off-specular scattering, Grazing Incidence Small Angle Neutron Scattering) are not

presented here but are extensively presented in the course devoted to it by Max Wolff in this thematic volume [6]. We will describe in the second part how it is possible to realize a NR experiment from practical point of view (description of instruments and of possible geometries of measurements, sample environments, accessibility to neutrons beams…). The third part is devoted to the presentation of some examples dedicated to the use of neutron NR for polymeric systems, with a specific emphasis on the different strategies of contrast variation that can be envisaged for such studies.

2 Principle of neutron reflectivity

The formalism described in this part is a wave formalism very close to the one usually used for reflection of light. It is limited to specular reflectivity and does neither consider the absorption of neutrons nor incoherent scattering.

2.1 Neutron-matter interaction and calculation of refractive index for neutrons

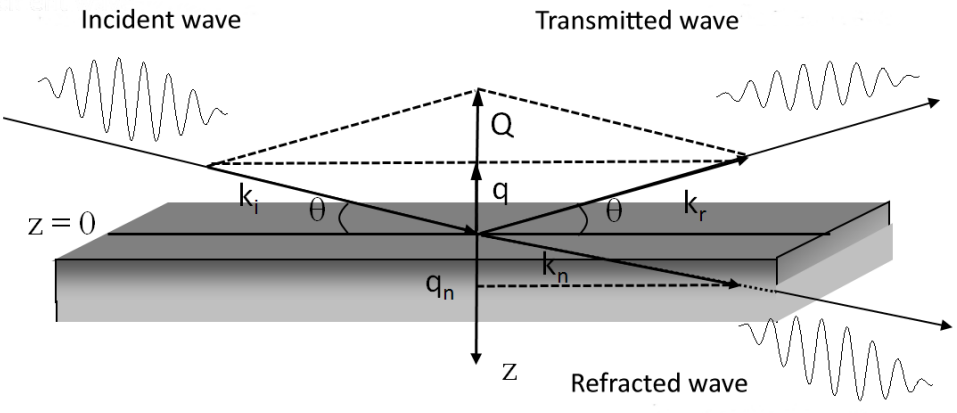

Figure 1. Reflection on an infinite planar surface.

Let us consider a neutrons beam reflecting on an infinite flat surface with an incident angle θ (see Figure 1). This surface is defined by the interface between vacuum (n=1) and a media with a refraction index n. In vacuum, the modulus of the wave vector of an incident neutron of wavelength λ is defined by:

$$k = \frac{2\pi}{\lambda} \quad (1)$$

The energy E of the neutron is:

$$E = \frac{\hbar^2}{2m} k^2 \quad (2)$$

where $\hbar$ is the reduced Planck constant and m the mass of the neutron.

In the media of refractive index n, the neutron interacts with the nuclei of atoms.
This interaction has a very short range and neutron-matter interaction is described by the Fermi pseudo-potential considering a point like potential V(r):

$$V(r) = b\left(\frac{2\pi\hbar^2}{m}\right)\delta(r) \quad (3)$$

where δ(r) is the Dirac function and *b* the coherent scattering length that describes the amplitude of interaction between neutron and the nuclei of the atom. This coherent scattering length has a real part and an imaginary part that accounts for absorption of neutrons by the nuclei. In the following *b* is always reduced to its real part because absorption is neglected. In the vacuum or in the media of index *n* the wave function ψ of the neutron is described by the Schrödinger equation:

$$\frac{\hbar^2}{2m}\Delta\psi(r) + [E - V(r)]\psi(r) = 0 \quad (4)$$

By considering that the structure of the media is invariant within the *xy* plan parallel to the surface, it is possible to separate the space variables *x*,*y* and *z* in equation (4) since V(r) is only dependent on *z*:

$$\frac{\hbar^2}{2m}\frac{d^2\psi_z}{dz^2} + [E_z - V_z)]\psi_z = 0 \quad (5)$$

The mean potential V_z within the layer is obtained by integration of the Fermi pseudo-potential:

$$V_z = \frac{1}{V}\int_V V(r)dr = \frac{2\pi\hbar^2}{m}Nb \quad (6)$$

where N is the number of atoms per volume unit.

In the framework of this course, one considers that neutrons do not exchange energy when then get reflected from the media of index *n* (**elastic scattering**). The conservation of energy at z = 0 enables to write the wave vector of neutrons in media k_n as a function of k and V_z:

$$\frac{\hbar^2k^2}{2m} = \frac{\hbar^2k_n^2}{2m} + V_z \quad (7)$$

One finally obtains from equation (6) and (7):

$$k_n^2 = k^2 - 4\pi Nb \quad (8)$$

This last equation allows to express the index of refraction *n* of the homogeneous media, defined as the ratio of the wave vectors in the material and in vacuum (6) :

$$n^2 = \frac{k_n^2}{k^2} = 1 - \frac{\lambda^2}{\pi}Nb \quad (9)$$

The product *Nb* is the **neutron coherent Scattering Length Density (SLD)**. Table 1 shows the coherent scattering length of some atoms and the SLD of some materials [7]. Please note that ***b* can be either positive or negative**, contrarily to the case of X-rays for which it is always positive and proportional to the number of electrons. Some full neutron tables of elements can be found on internet [8]. The SLD of the substrate is a crucial information in a NR experiment. It has to be ideally calculated prior to the experiment. Its calculation is very simple for crystals or solvents† but may raise difficulties for glasses

† An example of calculation of scattering length density: the case of water. This density is obtained through $Nb = (\Sigma_i b_i)/V$ where the b_i correspond to the atoms constitutive of the molecule (table 1) and V the volume of the molecule. Since the mass molar of H_2O is 18g/mol and the density of H_2O is 1g/cm^3, the volume of a molecule of water is $18/6.02\ 10^{23} = 2.99\ 10^{-23}$ cm^3 per molecule. The volume of a molecule of D_2O is the same. On gets :
$Nb(H_20) = (-0.374*2+0.58).10^{-12} / 2.99\ 10^{-23} = -0.56\ 10^{10}$ cm^{-2} (– 0.56 10^{-6} Å^{-2})
$Nb(D_20) = (0.667*2+0.58).10^{-12} / 2.99\ 10^{-23} = 6.38\ 10^{10}$ cm^{-2} (6.38 10^{-6} Å^{-2})

or polymers when the exact value of the specific volume of the molecule is not known with a high precision.

Table 1. Coherent scattering length of some atoms and scattering length density of some molecules. PS refers to polystyrene.

Coherent scattering length b (10^{-12} cm)					
^{1}H	D (^{2}H)	C	O	N	Si
-0.374	0.667	0.665	0.580	0.936	0.415
Scattering length density (Å^{-2})					
H_2O	D_2O	PS_H	PS_D	SiO_2	Si(crystal)
-0.56 10^{-6}	6.38 10^{-6}	1.41 10^{-6}	6.5 10^{-6}	3.41 10^{-6}	2.07 10^{-6}

The characteristic wavelengths of the incident neutrons being of the order of a few Å and the *Nb* of the order of 10^{-6} Å^{-2}, the values of the neutron refractive index *n* are always very close to 1 (~ 1± 10^{-3}). Contrarily to the case of visible light, **the effects of reflection/refraction for neutrons on surfaces occur only at very grazing angles, of the order of ~ 1°**. Please note that the refractive index can be smaller or larger than 1 for neutrons.

At the interface between the vacuum and the media of index n, one writes the refraction law of Descartes:

$$\cos\theta = n\cos\theta_n \tag{10}$$

Total reflection is achieved when $\theta \leq \theta_c$, where the critical angle θ_c is defined so that $\theta_n = 0$. If *n* is larger than 1, the conditions of total reflection are never fulfilled, which happens for example when the substrate is H_2O.

This leads to:

$$\cos\theta_c = n \tag{11}$$

The above equation is usually expressed as the sinus of the total reflection angle:

$$1 - (\sin\theta_c)^2 = 1 - \frac{\lambda^2}{\pi}Nb \tag{12}$$

Or equivalently:

$$\sin\theta_c = \sqrt{\frac{Nb}{\pi}}\lambda \tag{13}$$

When total reflection occurs, **the measurement of the critical angle θ_c for a given wavelength is a very precise measurement of the substrate's *Nb* and therefore of its chemical composition**.

2.2 Reflection on a succession of layers

The reflectivity is a function that is only dependent on the scattering vector $\vec{Q}$defined by:

$$\boxed{\begin{gathered}\vec{Q} = \overrightarrow{k_r} - \overrightarrow{k_\iota} \\ Q = \left\|\overrightarrow{k_r} - \overrightarrow{k_\iota}\right\| = \frac{4\pi\sin\theta}{\lambda}\end{gathered}} \tag{14}$$

It is equal to twice the projection of the incident wave vector k_i on the z axis perpendicular to the surface. In the following we will use in the calculation the variable q, projection of the wave vector on z such that q =Q/2.

If the system under study is made of several layers, each of them having a refractive index n_p, the plane wave functions describing the neutron within the layer p (ψ_p) and the layer p+1(ψ_{p+1}) can be written like:

$$\psi_p(z) = A_p \exp(iq_p z) + B_p \exp(-iq_p z) \quad (15)$$
$$\psi_{p+1}(z) = A_{p+1} \exp(iq_{p+1} z) + B_{p+1} \exp(-iq_{p+1} z) \quad (15')$$

where i^2=-1, and A_p and B_p are respectively the amplitudes of the wave propagating towards the inner and the outer of the material. From equation (8) we can also write:

$$q_p^2 = q^2 - 4\pi N b_p \quad (16)$$
$$q_{p+1}^2 = q^2 - 4\pi N b_{p+1} \quad (16')$$

The conditions of continuity of the wave and of its derivative at the interface p/p+1 are:

$$\psi_p(z_p) = \psi_{p+1}(z_p) = u(z_{p/p+1}) \quad (17)$$
$$\psi_p'(z_p) = \psi_{p+1}'(z_p) = u'(z_{p/p+1}) \quad (17')$$

The reflectivity at $z_{p/p+1}$ is defined by the ratio of the intensity of the beam reflected by the layer p+1 by the intensity of the incident beam on such a layer:

$$R = \frac{|B_p|^2}{|A_p|^2} = \left| \frac{1 - \frac{u'(z_{p/p+1})}{iq_p u(z_{p/p+1})}}{1 + \frac{u'(z_{p/p+1})}{iq_p u(z_{p/p+1})}} \right|^2 \quad (18)$$

where $u(z_{p/p+1})$ and $u'(z_{p/p+1})$ are functions that depend both on $z_{p/p+1}$ and q_{p+1}.

From this last equation it is possible to calculate the reflectivity at the last interface between the last layer and the bulk substrate material, and then to calculate recursively the reflectivity at each interface up to the outer surface in order to obtain the whole reflectivity of the system. This method is known as the optical matrix method that uses the Abeles formalism [9].

2.3 The ideal interface and the Fresnel reflectivity curve

Let us consider here a neutron beam propagating in vacuum (or air) and reflecting from an ideal planar substrate without any layer at the surface. If the interface is perfect without roughness, such a system is a diopter. The reflectivity of such an interface is called **the Fresnel reflectivity** (R_F). Its calculation can be achieved with last equation (18) by replacing the media p and p+1 by vacuum (n=1) and the substrate of refractive index *n*. In this case, within the bulk material substrate, B_{p+1}=B_s=0 in equation (15) because there is no intensity returning from z=∞. The Fresnel reflectivity writes:

$$R_F = \left|\frac{B}{A}\right|^2 = \left|\frac{q - q_s}{q + q_s}\right|^2 \quad (19)$$

or:

$$R_F = \left| \frac{1-\left(1-\left(\frac{q_c}{q}\right)^2\right)^{1/2}}{1+\left(1-\left(\frac{q_c}{q}\right)^2\right)^{1/2}} \right|^2 \quad (20)$$

where q_c and q_s are obtained from:

$$q_s^2 = 4\pi N b_s \quad (21)$$

$$q_s^2 = q^2 - 4\pi N b_p = q^2 - q_c^2 \quad (21')$$

q_c is the critical wavevector that separates total reflection (below q_c) from partial reflection where a part of the beam is refracted (above q_c). The measurement of q_c enables the measurement of Nb_s (this is another way of writing equation (13) in section 2.1).

Please note that, **far from the critical angle ($q>>q_c$), $R_F \propto (1/q)^4$**. This means that the decay of the reflectivity is always very steep whatever the layer at the surface (see the representation of figure 2 in linear scale). The NR curves R=f(q) are thus traditionally represented in linear-logarithmic scales or logarithmic-logarithmic scales, as in the inset of Figure 2. Another convenient way of representation is the *Fresnel representation* $R(q)q^4 = f(q)$ for which the q^4 term compensates the intrinsic q^{-4} decay of the NR curve to highlight the features coming from the layers at the interface (see the experimental data in the part 4 devoted to the examples). A last possible useful representation is to show $R(q)/R_F(q) = f(q)$.

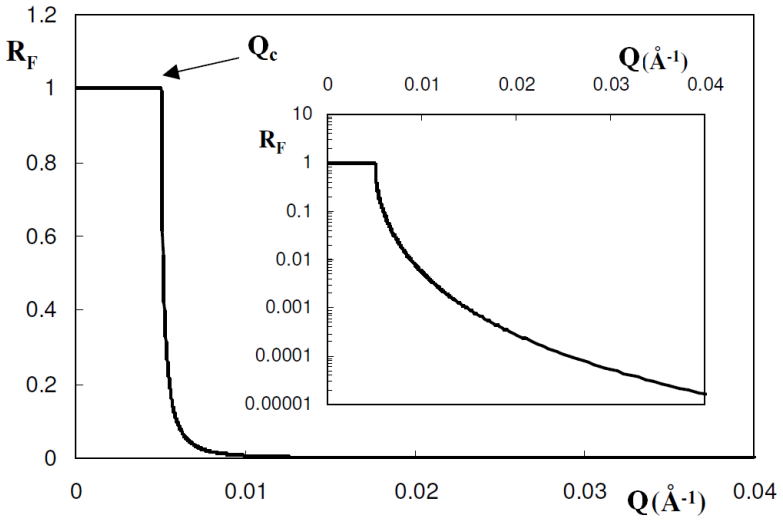

Figure 2 : Linear-linear representation and linear- logarithmic representation (inset) of the Fresnel reflectivity as function of Q for $Nb_s = 2.07\ 10^{-6}$Å^{-2} (interface air/silicon).

2.4 The case of an homogeneous layer on a substrate

Let us now consider that there is a single homogeneous layer of thickness *d* at the surface of the perfectly flat substrate whose thickness is considered as infinite (Figure 3). The three media are respectively the air (n=1), the layer of refractive index n_1 and scattering length density Nb_1 and the substrate of index n_s and scattering length density Nb_s. The air/layer interface is set at z=0 and the layer/substrate interface is set at z=d.

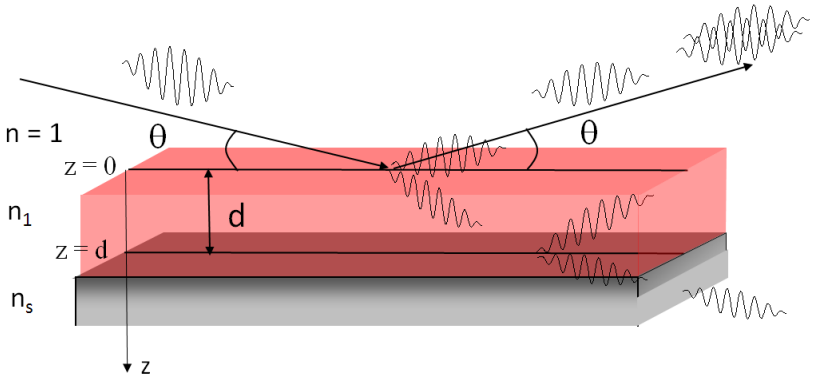

Figure 3. Homogeneous layer on a substrate.

On such a system a part of the incident wave will be reflected on the first interface at z = 0 and a part will be transmitted for $q>q_c$. Also a part of this last transmitted wave will be reflected on the second interface at z = d. The two reflected waves will interfere constructively or destructively depending on their phase which is directly linked to their difference of optical path and thus to the thickness of the layer. **It therefore appears qualitatively that the reflectivity curve will exhibit interference fringes that enable the measurement of the layer**.

After a few calculations the reflectivity writes:

$$R = \frac{\cos(2q_1 d)\left[1+\left(\frac{q_s}{q}\right)^2-\left(\frac{q_1}{q}\right)^2-\left(\frac{q_s}{q_1}\right)^2\right]+1-4\frac{q_s}{q}+\left(\frac{q_s}{q}\right)^2+\left(\frac{q_1}{q}\right)^2+\left(\frac{q_s}{q_1}\right)^2}{\cos(2q_1 d)\left[1+\left(\frac{q_s}{q}\right)^2-\left(\frac{q_1}{q}\right)^2-\left(\frac{q_s}{q_1}\right)^2\right]+1+4\frac{q_s}{q}+\left(\frac{q_s}{q}\right)^2+\left(\frac{q_1}{q}\right)^2+\left(\frac{q_s}{q_1}\right)^2} \quad (22)$$

It appears on such an equation that the curve of R as function of q will exhibit oscillations whose frequency is given by $2q_1 d = m \times 2\pi$ (m is an integer). This is the Bragg relationship corrected for the critical angle:

$$2d\sqrt{\sin\theta_m{}^2 - \sin\theta_c{}^2} = m\lambda \quad (23)$$

These oscillations are called the Kiessig fringes. The inter-fringes distance is linked to the thickness of the layer and their amplitude come from the difference of scattering length densities existing between the monolayer and both air and substrate. Figure 4 presents the characteristic NR curve of a system made of a single homogeneous layer on a substrate.

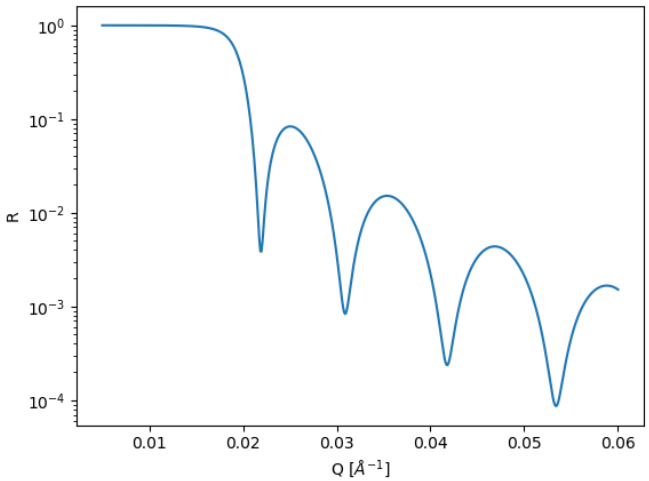

Figure 4. Reflectivity R calculated for a layer of deuterated PS (Nb=6.5 10^{-6}Å^{-2}) of thickness 500Å on silicon (Nb_s=2.07 10^{-6}Å^{-2}). The calculation has been done by taking into account an experimental resolution, assuming a typical resolution of neutron reflectometer (see part 3.1).

2.5 Roughness and interdiffusion

Up to now, we have considered that the interface between the layer p and the layer p+1 was perfect without any heterogeneity. There was thus a discontinuity in Nb(z) when passing from Nb_p to Nb_{p+1} (step function). In practice, the interfaces are never so abrupt because of two different physical phenomena: *(i)* the **roughness** and/or *(ii)* **the interdiffusion** (see Figure 5). The roughness accounts from the fact that the passage from one layer to the next is not always at the same distance from the surface z from one area of the surface to another. The interdiffusion accounts from the fact that two materials making two successive layers often mutually diffuse slightly one to each other, which creates a smooth transition.

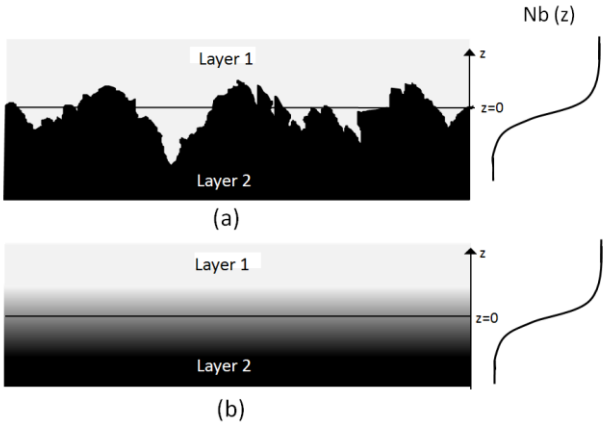

Figure 5. (a) Schematic representation of roughness; (b) schematic representation of interdiffusion. The profiles represented on the right show the effective Nb(z) profile averaged over the whole surface.

The lone measurement of the specular reflectivity does not allow to distinguish between roughness and interdiffusion. If the size of the defects is smaller than the spatial coherence length of the neutrons (of the order of a few micrometers), off-specular measurements allow to discriminate between the two cases. Roughness is indeed equivalent to have reflections by numerous surfaces with different angular

orientations which make some neutrons being reflected out of the specular plane. This does not happen in case of interdiffusion.
Assuming that both kinds of interfaces have a Gaussian profile, they will be simulated by the same error function:

$$erf\left(\frac{z-z_{p/p+1}}{\sigma_{p/p+1}}\right) = \frac{2}{\sqrt{\pi}}\int_0^{(z-z_{p/p+1})/\sigma_{p/p+1}} e^{-t^2}\,dt \qquad (24)$$

where p/p+1 is the interface between two successive layers. The curve that shows such an error function has an inflection point in $z_{p/p+1}$. $\sigma_{p/p+1}$ is the inverse of the tangent's slope of the curve at $z_{p/p+1}$. The thickness of the interface is given by $2\sigma_{p/p+1}$.
It is possible to show that the introduction of such roughness is equivalent to multiply the reflectivity R obtained in case of a perfect flat interface between p and p+1 (equation 19) by a Debye-Waller factor that writes:

$$DW = \exp(-4q_p q_{p+1}\sigma_{p/p+1}^2) \qquad (25)$$

where q_p and q_{p+1} are given by equation (16). This approach is only valid when the roughness is smaller than the thicknesses of the adjacent layers and the lateral fluctuations of the roughness are smaller than the coherence length of the beam.

Another method to take into account roughness is to discretize the density profile in a large number of layers having a low variation of the *Nb* from one layer to another. However, the calculation time may become very long.
Figure 6 shows the effect of roughness/interdiffusion on the NR curve calculated in case of the single layer reflectivity of deuterated PS of thickness 500Å on silicon substrate already presented in Figure 4.

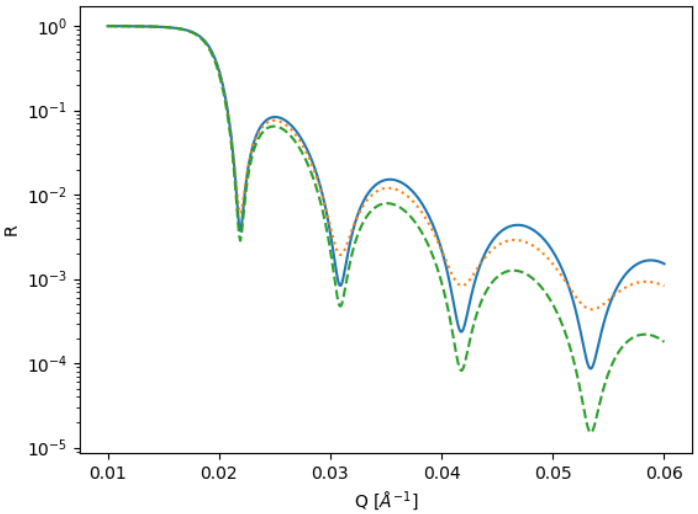

Figure 6. Influence of the roughness on the NR curve calculated on a 500Å deuterated PS deposited on a silicon substrate. Thick line: $\sigma_s = \sigma_{air} = 0$Å; dashed line: $\sigma_s > 0$; Dotted line: $\sigma_{air} > 0$. The calculation has been done by taking into account an experimental resolution, assuming a typical resolution of neutron reflectometer (see part 3.1).

2.6 Data modeling

2.6.1 Calculation of a reflectivity curve

As mentioned in paragraphs 2.2 to 2.4, **it is possible to numerically calculate recursively the reflectivity of a system with n layers if the thickness and the scattering length density of each layer is known, taking into account the roughness at each interface between two adjacent layers** by the optical matrix method. The data modeling is then achieved by fitting numerically the calculated NR curve to the experimental curve. The parameters of the fits are the respective thicknesses and scattering length densities of the layers of the multilayers system probed, as well as the roughness of the interfaces. The experimental resolution has also to be taken into account in the calculation (see paragraph 3.2). When the scattering length density profile perpendicular to the surface Nb(z) is continuous (as in the case of the adsorption profile of a polymer in solvent at an interface for example), such profile can simply be discretized. The scattering length density of a layer that contains several types of objects is the average of the scattering length density of the objects weighted by their volume fraction within the layer. It is assumed in this case that the average on the coherence area of the beam is representative of the average of the SLD on the whole surface. For instance, in the case of a two-phase layer made of polymers in a solvent, the *N*b of the layer is $Nb(\text{layer}) = \Phi_{poly}\, Nb_{poly} + (1 - \Phi_{poly})\, Nb_{solvent}$.

2.6.2 Data fitting

Although the calculation of a NR curve from a known profile is easy, the fitting of NR is in fact tricky. This stems from the fact that the NR curves cannot be inverted in direct space because only the intensity is measured and not the phase. **Therefore different profiles in direct space may give the same NR curve**. Besides, owing to the rather poor fluxes provided by the neutron sources, the error bars are often rather large in an experiment, which makes the distinction between two close profiles sometimes impossible. A blind treatment of the raw data by a fitting program that will minimize a χ^2 between calculated and experimental NR curve starting from a random profile is thus very risky, as it can converges towards a non-physical profile. It is thus important to start with a reasonable physical profile. In particular, the SLD of the different components of the systems have to be evaluated prior to fitting when it is possible in order to constrain the parameters of the fit, or at least to mark them off. Then, it is mandatory to check that the obtained profiles are consistent from a physical point of view. For instance, when studying a responsive thin polymeric layer as function of a stimulus, mass conservation has to be verified (see for instance the example presented in part 4.3). Ideally, results have to be confronted with complementary results obtained with other techniques (isotherms, QCM, etc..). This sometimes enables to discriminate between several possible profiles.

There exists also a very popular strategy to obtain unambiguous results based on a specificity of NR from the contrast point of view. It consists in achieving the experiment by using several different neutron contrasts for a given physical profile. For instance, when probing a thin solvated organic layer at the air/liquid or solid/liquid interfaces, the SLD of the solvent can be easily changed by total or partial deuteration. At the present times, most studies performed at the air/water interface involve at least 3 different contrasts conditions for the aqueous subphases (H_2O, D_2O and a mixture of both). Obtaining of a unique profile that fits all experiments simultaneously in the different contrasts conditions enables then to assess the real profile with confidence [1]. This strategy have some minor drawbacks, namely the necessity to make reproducible samples in various contrast conditions as well as the possible change of physical properties of the system upon deuteration, that generally only occurs when H-bonding plays an important role.

There exists also another experimental strategy to refine modelling based on the insertion of a magnetic layer below the layer to be studied and to perform polarized NR. The advantage here is to get two contrasts conditions on a unique sample but the price to pay is the addition of a layer that make the system more complex [10], that can however be fully precisely characterized by X-Ray reflectivity prior to neutrons, and the use of polarized neutrons that decrease the flux. Although very elegant, this strategy has only be very sparsely used in literature.

3 Experimental aspects of neutron reflectivity measurements

3.1 Instruments

3.1.1 The Different kinds of instruments

There exists two ways to measure the reflectivity of a sample as a function of the scattering vector $Q = 4\pi\sin\theta/\lambda$ (see Figure 7).

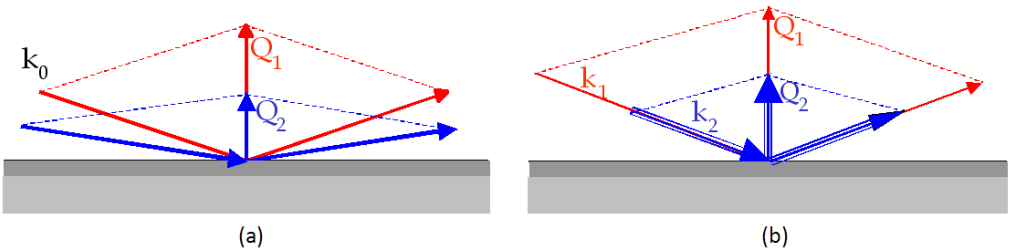

Figure 7. Principle of neutron reflectivity: (a) θ, 2θ: measurement at variable θ and fixed λ; (b) time of flight: measurement at fixed θ and variable λ.

The most simple **(θ, 2θ)** is similar to a 2-axis diffractometer and uses a fixed wavelength λ, that typically lies between 1.5Å and 6Å. It is perfectly suited to reactors that provide a continuous neutron flux. The neutron beam, polychromatic at the reactor source, is made monochromatic upstream of the sample by a monocrystal, collimated, and sent on the sample in grazing incidence. One measures then the reflected beam, step by step, by rotating the sample to an angle θ and the detector of 2θ, similarly as in a diffraction 2-axis experiment. The illumination of the sample varies from one angle to another and has to be taken into account in the data reduction. Such a geometry is also used for measurements with X-rays.

The relatively low neutron velocities allow to use another method of measurement called **time of flight** to measure NR curves, enabling to work at fixed θ and to measure as a function of λ. This method is especially suited to pulsed sources (spallation sources) and is so convenient for NR that it is very often used with reactor sources, too. The neutron moves at a finite speed, linked to its wavelength *via* the De Broglie relation $v = h/m\lambda$ where h is Planck constant and m the neutron mass. For the cold neutrons used in the experiments (with a typical wavelength that ranges between 2 and 20 Å), the speed of neutrons lies between a few 100 m/s and a few 1000 m/s. This permits to determine the wavelength of a given neutron within a polychromatic neutron beam by separating the neutrons of different wavelengths of a neutron pulse through their speed, the fastest neutrons moving faster than the slower ones. The pulse, which is spontaneously created on a spallation source, is created by a chopper on a reactor source. The neutrons beam is sent in grazing incidence on the sample and the chopper defines the origin of times $t_0 = 0$ (the "starting line"). One measures then the time t taken by the neutron to reach the detector located at the distance L from the chopper to determine the wavelength (via $\lambda = h/mL*t$)[‡]. The rotation of the chopper is chosen so that the slowest neutrons of a pulse arrive sooner on the detector than the fastest neutrons of the next pulse in order to avoid the overlap of the pulses. In some setups, an other chopper is placed upstream of the beam to avoid this "frame overlap", which makes it possible to

[‡] One recalls that the value of the Planck constant h is $6.62\ 10^{-34}$ J.s and that the value of the neutron mass is $1.67\ 10^{-27}$ kg. The expression can then be rewritten like λ(Å) = t(μs)/(252.7*L(m)). The travel time is then around 1ms/Å. With a flight path length of a few meters, it is possible to discriminate neutrons with a very good resolution with conventional electronics. For instance, on EROS spectrometer at LLB, it was possible to distinguish between neutrons whose wavelength varied from 0.2 Å by counting neutrons by slices of 200 μs with electronics with the flight path of 4.4m.

increase the speed of rotation of the first chopper and in turn to increase the flux on the sample for the longest wavelength. Measuring the coefficient of reflection is simple: The white incident polychromatic beam has to be first determined by measuring the incident beam directly on the detector without any reflection. The intensity measured for the reflected beam has then to be divided by this incident white beam for every value of λ.
The time-of-flight method is extremely convenient for some geometries of measurement, in particular those at the air/liquid, because it does not force to rotate the sample (and to make it flow…). Moreover, it enables to measure all the points of a reflectivity curve at the same time, or at least one decade in q, which removes any incertitude on the possible aging of the sample during measurement, a feature that often occurs in soft matter. Along the same lines, this method allows **kinetics measurements** that have become very popular these last years with the development of high-fluxes reflectometers such as Figaro at ILL that enable to measure a given NR spectrum in a few minutes [11].
In an NR experiment, the incident angle on the surface to study is always very small, ranging typically from 0.5 to 5°. Given the typical wavelengths of the incident neutrons (~ 3Å-25Å), the range of scattering vectors lies between 0.003 $Å^{-1}$ and 0.3 $Å^{-1}$. The typical thicknesses that can be measured in standard conditions vary then from around 10 Å to 2000 Å.

3.1.2 An example of Time-of-Flight Spectrometer: EROS at LLB

A full description of this horizontal spectrometer can be found in reference [12]. It is shown on Figure 8. Briefly, the neutrons produced by the Orphée reactor (CEA Saclay) are thermalized by a liquid hydrogen cold source (T=20K). A bended neutron guide conveys them up to the spectrometer located at around 30m from the source. A "white" beam containing a broad spectra of wavelengths is then available at the chopper position (in practice from 3 to 25Å). The chopper with a raw δλ/λ constant resolution is made of two-rotating wheels covered by gadolinium, a neutron absorber, pierced by two large slits. The distance and phase between the two wheels enable to change the δλ/λ from 1% to 13% depending on the resolution request. The beam passes then through a collimator under vacuum that is 1.8m long. The aperture of the horizontal entrance and exit slits can be opened from 0.2 mm up to several cm (in standard conditions, one uses apertures lying from 1mm to 3mm). Two neutron supermirrors can be inserted within the collimator to deviate the beam for air/liquid measurements. The beam is then reflected by the sample tilted of an angle θ and measured by a ^{3}He single detector.
The maximum angle that can be reached is 5°, which enables to cover scattering vectors ranging from 0.003 to 0.3$Å^{-1}$ (measurements below 0.3° are practically almost impossible because the reflected beam has to be separated from the incident non-deviated direct beam). A measurement at one angle allows to cover around one decade in q. Sometimes this is sufficient for the desired measurement, however, in most cases 2 or 3 different angles are used to cover a broader q-range. The actual minimal reflectivity in air/solid geometry that can be obtained is typically R ~ 10^{-7}. For measurements involving liquids, this limit is superior to 10^{-6} because of incoherent scattering (see reference [12] for more details). The vertical position has to be adjusted as a function of the chosen angle. If h_0 are h_D are the respective position of the direct beam and of the detector at the distance L from the chopper, the angle of a measurement θ is given by: $\tan 2\theta = \frac{h_D - h_0}{D_{S\_D}}$ where D_{S_D} is the distance from the sample to the detector (figure 8).
The principle of alignment is simple. The angle of work has to be chosen first such as a part of the neutron beam is in total reflection (if the neutron contrast conditions enable it) thanks to the formula (13). The height position is then fixed. The sample has then to be placed within the beam and rotated with the goniometer up to recording the maximum of neutrons on the detector. This is exactly similar to what children do when they rotate their watch to reflect the light (the neutrons) in the eye of someone (the detector)… For air/liquids measurements, the angle of work is fixed by the deviating supermirrors within the collimator (see Figure 8.b).

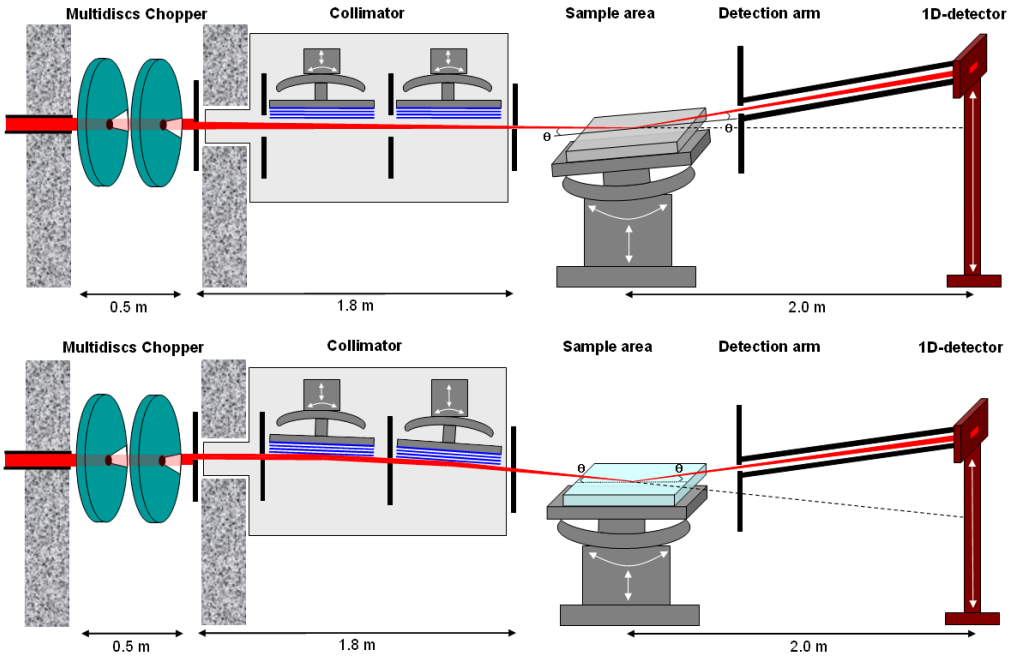

Figure 8. Scheme of the EROS reflectometer, from reference [12]. Top: Geometry for air/solid measurements; Bottom: Geometry for air/liquid measurements.

The typical duration of the acquisition time depends on the minimal reflectivity that is requested. If it is of the order of 10^{-5}, 30 min to 1h are necessary to obtain a correct statistics but this time has to be extended up to ~ 4 hours to reach a few 10^{-6}. These typical measurement times are given for sample of around 10 cm². Such large surfaces can be indeed used because the collimations used are large (see below).

3.1.3 Angular resolution

Owing to the collimation, the incident beam on the sample has a divergence δθ that induced an enlargement of the beam and that has to be taken into account in the calculation, the expressions presented in the precedent part for the reflectivity being calculated for an incident beam without divergence. This is achieved by the convolution of the calculated function by an apparatus function $f(\theta,\delta\theta_0)$ centered in 0. This function can be either a triangle function or a square function.

$$R_{\delta\theta/\theta}(q) = \int R\left(q\frac{\sin\theta_0}{\sin\theta}\right) f(\theta_0 - \theta, \delta\theta) d\theta \qquad (26)$$

The divergence of the incident beam δθ and the angular resolution δθ/θ are set by the apertures of the entrance and exit slits of the collimator and by the collimator length D_c. If the earth gravity is neglected, the trajectory of the beam is supposed straight and the divergence by: $\tan\delta\theta = (S_{ent}+S_{exit})/2D_c$. The calculation of the resolution for an angle of 1°, for slits S_{ent} = 2 mm and S_{exit} 1mm and for D_c=1800 mm give : δθ= 0.047° and δθ/θ = 4.7% (characteristic values used on EROS).

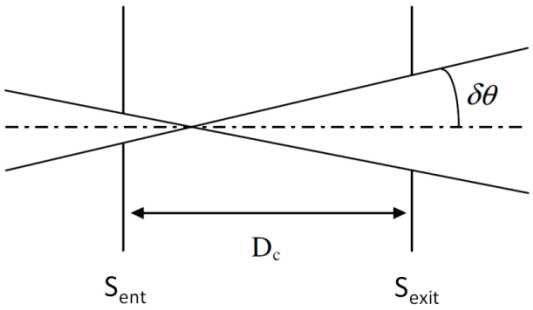

Figure 9. Divergence of incident beam when the effect of the earth gravity on the neutrons path is neglected.

3.2 Samples and possible geometries of measurements

The geometry of a neutron reflectivity experiment imposes three imperative conditions that have to be absolutely fulfilled to make it feasible. First, the media in which the neutron beam is travelling upstream the interface and after reflection has to be totally or partially transparent to neutrons, otherwise signal is lost. Second, **the flatness of the interface to be probed has to be as best as possible**, otherwise if it has a curvature this would have an effect equivalent to an increase of the divergence δθ of the beam. Although this divergence could be taken into account by an increase of the effective δθ within the resolution function during the data modeling, it has to be as limited as possible. This imposes some limitations on the different possible geometries of measurements and on the samples themselves. Third, the roughness of the surface has to be very limited, otherwise it would induce a very steep drop of reflectivity that leads to a loss of information on the scattering length density profile.

3.2.1 The different possible geometries of measurements

In soft matter, four types of interfaces are interesting to be studied: **air/solid** (spin-coated monolayers, polymeric nanostructures, etc..), **air/liquid** (surfactants monolayers, adsorption behavior of hydrophobic compounds, etc..), **solid/liquid** (polymeric brushes in solvent, interactions of biological species with membranes deposited on solid substrate, etc…) and **liquid/liquid** interfaces (model systems mimicking oil/water interfaces found in emulsions, etc..).
Air is almost transparent to neutrons. Indeed, the attenuation of a neutron beam for the wavelengths used is of the order of a few percent per meter. The length of the sample stage being of the order of a few tens of centimeters on a NR spectrometer, this attenuation is negligible when working in air/solid or air/liquid geometries. These two geometries are thus very easy to implement (figure 10).
Conversely, the transparency of media in which the neutron beam is travelling is a key point to consider for measurements in solid/liquid or liquid/liquid geometries (considered here as either water or an organic solvent as found in typical *Soft Matter* systems). In practice, two processes attenuate the beam: absorption and incoherent scattering. As mentioned earlier, only a very few atoms of the periodic table [7] have an important cross-section of absorption (^{3}He, ^{6}Li, B, Gd…), therefore absorption usually never hampers the design of an experiment. It has thus to be checked prior to the experiment that such atoms are not present in large amounts in the sample. On the contrary, incoherent scattering is a real problem to deal with when designing experiments. Incoherent scattering is a scattering that occurs with a constant probability over 4π independently from the position of scatterers (see introduction courses on neutron scattering for more information). For a given atom, the incoherent scattering cross-section comes from the different isotopes of the element and its different spin states. It is null or very weak for most elements of the periodic table, but unfortunately, rather important for ^{2}H deuterium and very high for hydrogen

$^{1}H^{\S}$. The incoherent scattering of a liquid is thus very important, which in turn decreases the transmission of the beam. For example, the transmission by a neutron beam at $\lambda = 6$ Å is only 0.5 through 1 mm of H_2O and 0.8 through 2 mm of D_2O. As the neutron beam has to travel on several centimeters in a NR experiment within the sample because angles of incidence are grazing (less than 5°), crossing a liquid is almost impossible. For measurement in solid/liquid geometries, the poor transmission of liquid is easy to circumvent. The neutron beam has simply to pass through the solid as shown in figure 10.c, provided that the solid chosen is transparent to neutrons, which is easy to achieve with silicon wafers (see next section) or quartz crystals. Such geometry of measurement is thus very wide spread in experiments related to Soft Matter.

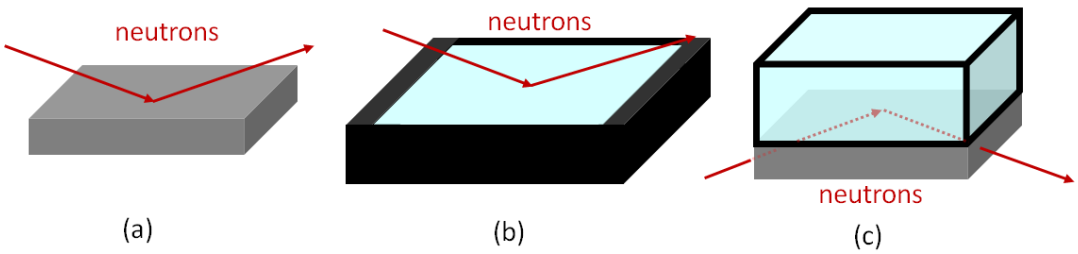

Figure 10. Standard geometries of measurements in Neutron Reflectivity: (a) air/solid interface; (b) air/liquid interface; (c) solid/liquid interface.

For **liquid/liquid geometries**, there are not good solutions and measurements are very sparse. Historically, the first strategy used to overcome the problem was to work in *pseudo* air/liquid geometry by using a ultrathin oil layer of well controlled thickness of ~ 3000 Å on water surface to probe a surfactant layer sandwiched between oil and water [13]. The limited loss of neutron through the oil made the experiment possible. Very nicely, the use of an hydrogenated surfactant and deuterated oil and water of same SLD enabled the determination of both the thickness and the roughness of a surfactant layer at the interface.

Later, the same kind of strategy was adapted at the solid/liquid interface. A thin uniform oil layer was trapped between a solid substrate and a bulk aqueous subphase. The thin oil layer was first spread onto the surface by a spin-coating deposit, then frozen below its melting temperature, sandwiched between the solid and the water, and maintained after thawing the oil phase [14].

Finally, true liquid/liquid measurements are now emerging owing due to gain performances of the present reflectometers compared to those operating thirty years ago. For instance, in reference [15], water-toluene interface was probed in a cell specifically designed for the purpose. The beam crossed a sapphire before travelling through several hundreds of microns of water before hitting the toluene interface. The SLD of water was adjusted to those of sapphire, so the first sapphire/water interface that was reached by neutrons was transparent to them. Such measurements remain however very tricky, in particular obtaining a flat interface over a large surface between two liquids is very difficult. In the above mentioned cited example, the cell was designed so that the lower part was hydrophilic and the upper part was hydrophobic, so as to force the interface between the two liquids.

§ We regret here that ^{1}H has a very high incoherent scattering cross-section (80 barns) for what concerns neutron reflectivity. It has however to be noted that it is a true advantage in other neutron techniques such as quasi-elastic and inelastic scattering (see for example the course of Berrod *et al* in the current volume for more information [34]).

3.2.2 Samples

Besides the required qualities of transparency towards to neutrons depicted previously, it is mandatory that samples fulfill other conditions.

First, the surface of the sample has to be optimized. In practice, the raw measured reflectivity is directly proportional to the surface of the sample illuminated by neutrons, prior to the data reduction step where it is normalized to unity for total reflection. If possible, the surface of the sample has to be maximized in order to get a good signal-to-noise ratio with reasonable acquisition times. Ideally, the best is to have an overall surface of sample that is higher than the area illuminated by neutrons during experiment (some cm^2 depending on the collimation and samples). The surfaces can be decreased at cost of increasing counting rate but one must avoid to decrease surfaces area down to 1 cm^2.

Moreover, when a sample is studied at the air/liquid interface, it is necessary that the surface of the sample is sufficiently large so that the beam illuminates a perfectly flat area of the surface, thus located away enough from the edges (meniscus). This might be a problem if one studies the adsorption of an expensive molecule at such an interface because a minimal quantity is required.

Second, for solid samples, the surface curvature has also to be considered. It is indeed mandatory that such samples are rigid enough not to deform mechanically under internal stresses and have a very small *rms* roughness. Most common solid substrates used in neutron reflectometry are sapphire, quartz crystals and silicon wafers. These latter are especially suited to design model substrates for NR and are used in ~90% of experiments on solid substrates in soft matter, both at air/solid interface and solid/liquid interface because they have several properties that make them unique for NR: *(i)* they are nearly transparent to neutrons because their incoherent scattering cross-section is null and their absorption cross-section is very weak (7 cm of silicon are required to attenuate a neutron beam at $\lambda = 6$Å by a factor 2 !); *(ii)* their lack of incoherent scattering do not produce any additional background scattering; *(iii)* they have an excellent mosaicity with an *rms* roughness of a few Å; *(iv)* their chemical surface (Si-OH groups) lends itself to many chemical modifications which are easy to achieve at laboratory without any specific material in order to design hydrophilic surfaces, hydrophobic surfaces, charged surfaces, functionally-terminated surfaces...; *(v)* last but not least, they are rather cheap and easy to purchase at silicon manufacturers owing to their importance in electronic industry.

Third, one must also ensures that samples do not contain atoms that strongly absorb neutrons (Li, B, Gd…) or have an important incoherent scattering cross-section (V...) to avoid the decrease of flux in general and the radiological activation of samples in case of absorption. This is especially important for the solid incoming media that has to be crossed in solid/liquid geometries.

3.2.3 Sample environment

Thanks to the poor absorption of neutrons by matter and in particular by some metallic elements, it is easy to design various samples environments for *in situ* experiments: liquids cells, cells with solvent circulation baths, Langmuir trough, ovens, pressure cells, temperature controllers, etc.. It is advised to contact people from facilities prior to experiments to check that the equipment can be used with the kind of sample to study or to design a dedicated sample environment for a specific experiment.

3.3 Access to the existing reflectometers

As NR is a growing expanding technique, there are reflectometers in all of the large neutron facilities. A state of the art of new offers on reflectometry has been described in a recent special issue dedicated on neutron instrumentation that focused on the reflectometers recently released or upgraded, as well as the new techniques of instrumentations in NR [16]. In France, there exist two neutron facilities, the European source *Institut Laue Langevin* (ILL) located in Grenoble [17] and the French national source *Laboratoire Léon Brillouin* (LLB), located in Saclay 30 km from Paris [18]. There are actually 3 reflectometers at ILL (FIGARO dedicated to soft matter and biophysics, D17 for multipurpose measurements and SUPERADAM for magnetic studies) and 2 at LLB (HERMES, a horizontal versatile multipurpose instrument, and PRISM for magnetic studies). In the near future, the new *European*

Spallation Source will be operating. Two reflectometers are planned: KESTIA, a vertical polarized reflectometer that should be opened to users in mid-2023 and FREIA, a high flux horizontal reflectometer very suited to soft matter that is forecast for 2025 [19]. All of these instruments are available free of charge to the whole scientific community. The beamtime is allocated by a committee of experts on the basis of experimental proposals that can generally be submitted twice a year. Please visit the websites of the facilities for all information on formalities. Fast access or paying beamtime for industrial applications for which data have to remain confidential are also possible. The beamtime must then be negotiated directly with the facilities.

4 Examples of use contrast variation in neutron reflectivity for soft matter

Over the last 30 years, the unique properties of neutron reflectivity revealed to be an invaluable and an indispensable tool for the study of *Soft Matter*, in particular for the study of surfactants, polymers, adsorption of binary mixtures and membranes. This abundant literature has given rise to numerous reviews since the famous ones by Penfold and Thomas on surfactants [1] and those by Russel on polymers in the early 90's [2], for instance those on solid/liquid measurements [4] or on supported membranes [3][20]. We thus do not aim here to make a review on the topic, and we refer back to the existing ones. Among the very recent ones, those by Naranayan *et al* is very comprehensive [21] and those by Braun *et al* is very complete on possible experiments at the air/water interface [22]. In the following, we present some examples that depict the strategies based on contrast variation that can be used in neutron reflectivity, in order to guide the reader to design his/her own future experiments. We have selected some examples on polymers but they are generally transposable to other fields of *Soft Matter*.

4.1 Nanostructured polymer thin films

There is nowadays a strong interest in polymer science in developing nanostructured thin films from the layer-by-layer (LBL) technique. This technique consists in depositing alternatively and cyclically two (or more) thin layers of polymers or nanoparticles that interact one with each other to design nanomaterials with a high output value. The initial coating processes involved dip coating and has been extended to spray. For all these processes, the interaction between adjacent layers (electrostatic, hydrogen bonding.) play a significant role. Two important questions have to be answered when designing such multilayered system: Is the final system really nanostructured after synthesis, or is it partially or completely interdiffused? If the system is really nanostructured, does it keep such nanostructure when immersed in a solvent? NR combined with contrast variation is the best technique to answer such questions owing to the possibility of probing buried interface, especially when both components are polymers, as in most cases. Usually the elementary polymer layer is very thin, typically 10-20 Å, so it is not possible to distinguish the two kinds of polymers within the architecture, whether they are both hydrogenated or deuterated, because there exist always partial interdiffusion between adjacent layers. Only the overall thickness of the layer is then measured. On the reverse, if one of the two polymers is deuterated at regular intervals, it is possible to assess if the system is truly nanostructured. There are then 3 typical sizes in the system, which are easy to decouple if the experimental sample has been intelligently conceived: the thickness of the deuterated layer, which enables in particular to estimate the typical range of interdiffusion of a polymer layer with the adjacent one, the distance between two deuterated layers and the overall thickness of the multilayered system. This is illustrated in figure 11 that shows some data obtained on a poly(styrene sulfonate) (PSS)/poly(allyl amine hydrochloride) (PAH) multilayered system obtained by spray coating [23]: the

top panel shows data when both PAH and PSS are hydrogenated. Only the Kissieg fringes associated with the overall thickness are visible. Conversely, when some of the PSS layers are deuterated, Bragg peak and its harmonics appear, revealing the true nanostructured nature of the system (lower panel). Please note that Decher has used such an approach to demonstrate that the LBL technique allows to make very well defined nanostructures in his very famous seminal paper on the topic[24], which is maybe the most cited paper ever published on soft matter that contains neutron scattering experiments**.

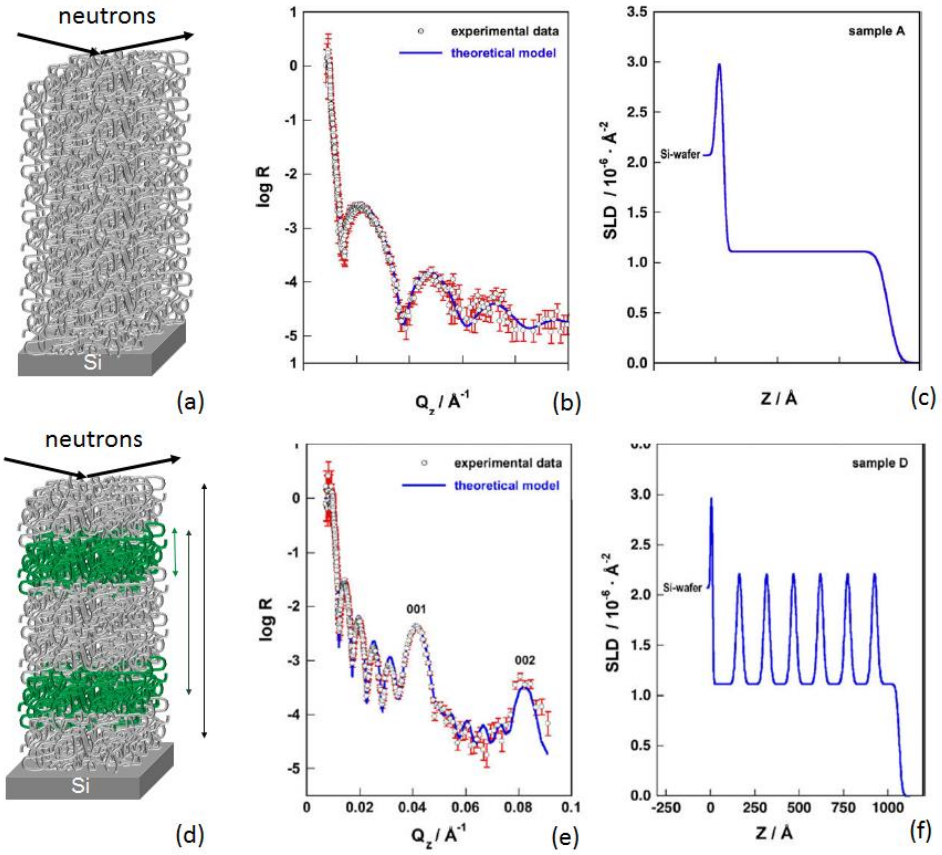

Figure 11. Top panel: structure of a nanostructured PSS/PAH polyelectrolyte multilayers when both polyelectrolyte are hydrogenated. (a) Sketch of the system from neutron contrast point of view; (b) Experimental neutron reflectivity obtained curve and fit with the SLD profile presented in (c) [23]. Lower panel: structure of a nanostructured PSS/PAH polyelectrolyte multilayers when the targeted architecture is: $[(PSS_{H7}/PAH)_5/(PSS_{D7}/PAH)_1]_6/(PSS_{H7}/PAH)_5$. (d) Sketch of the system from neutron contrast point of view; (e) Experimental neutron reflectivity obtained curve and fit with the SLD profile presented in (f)[23].

4.2 Dense brushes: growth of polymerization

Playing with contrast also allows to get an insight on a polymerization process. The idea is to change the contrast during the process so that the system keeps a "memory" of the process from the contrast

** At the date 8/2018, there are more than 7500 citations in Isi Web of Knowledge or more than 9500 in Google scholar.

point of view after its synthesis. This is illustrated here on the characterization of a PS brush grown on a silicon wafer through a *grafting from* approach were both the grafting density σ and the polymerization index N were precisely tuned [25]. The grafting density σ was controlled thanks to the deposit onto the surface of a monolayer of initiators which density was adjusted by Langmuir-Blodgett techniques. The polymerization index N was controlled by the NMP controlled radical polymerization technique. Such a technique enabled to obtain brushes with a very large range of densities up to a record of 1.1 chains/nm^2 [26]. NR was then used to demonstrate that all chains truly grow simultaneously in order to prove that the polymerization process was really controlled. To this aim, a brush was grown in two distinct steps: the brush was firstly initiated by deuterated monomers, stopped and then initiated again with hydrogenated monomers. Finally, although the brush was homogeneous from chemical point of view, it is an H/D di-bloc copolymer from the contrast point of view (figure 12.a).

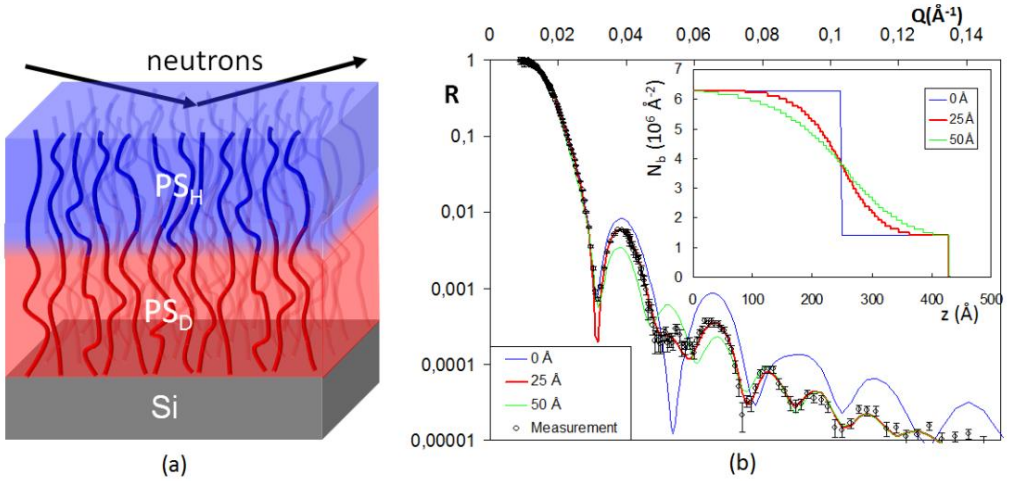

Figure 12. Dense brushes of Polystyrene grown initially by deuterated monomers and re-iniated by hydrogenated monomers [26]. (a) Sketch of the system from neutron contrast point of view at the end of the polymerization process; (b) Comparison between the NR curve obtained experimentally and the simulated curves corresponding to the different SLD profiles presented in inset.

The measurement of the interdiffusion layer between hydrogenated and deuterated parts enabled to probe the efficiency of the control of the polymerization. The NR reflectivity curve shows irregular interferences fringes (figure 12.b). This comes from the fact that there exist three distinct thickness within the system: those of the whole brush (420 Å), that can be measured independently by ellipsometry as the PS layer is homogeneous from optical refractive index point of view, those of the deuterated part (270 Å) and those of the hydrogenated part (150 Å). If there were no interdiffusion in the system, the NR signal would be completely dominated by the deuterated part since the PS$_D$/air contrast is much larger than the PS$_H$/air contrast. One would obtain almost regular fringes whose *d*-spacing would allow to recover the thickness of the deuterated part (simulation in blue in figure 12.b). Conversely, in case of a very large interdiffusion, one would only measure the typical reflectivity curve of the overall layer. The fringes would then again been regular but with a much larger *d*-spacing (simulation in green in figure 12.b). Between these two limit cases, a very weak variation of the interdiffusion layer strongly modify the reflectivity curve, especially when the interferences resulting from the deuterated layer and the whole layer are phase opposite, which induced the partial or total extinction of the fringes (see for example around 0.05 Å^{-1}). This enables a very precise determination of the thickness of the interdiffusion layer because some fringes appear or disappear upon variation of the thickness of a few Å. The obtained value from the best fit of the NR curve (25Å) is much smaller than the overall thickness, which proves that the polymerization approach was very efficient.

4.3 Behavior of thin polymer films in solvent

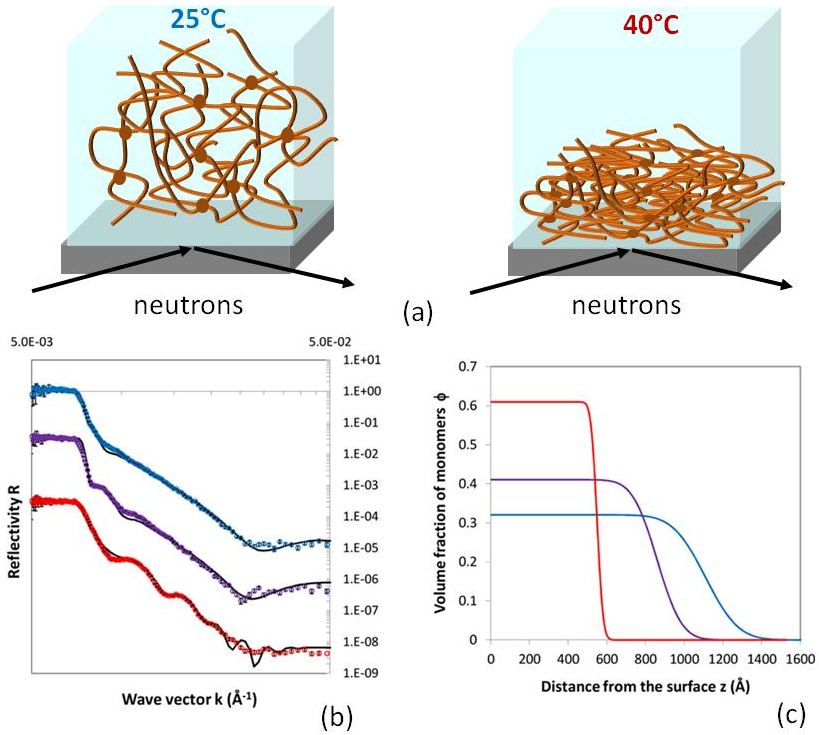

Figure 13: Aqueous behavior of a cross-linked hydrogel based on a thermo-sensible polymer (PNIPAM) tethered on a solid surface [27]. (a) Sketch of the system in two situations, respectively below the LCST (25°C, left) and upon the LCST (40°C, right); (b) NR curves corresponding respectively to 25°C (blue), 34°C (purple), and 40°C (red). The curves are shifted in intensity for clarity. (c) Volume fraction profiles corresponding to the best fits of the curves presented in (b).

One of the major actual trend in *Soft Matter* is the design of so-called *smart* materials, or more precisely stimuli-responsive materials, whose macroscopic properties can be tuned over a large range on demand in a controlled manner triggered either by a small change of environment (temperature, pH) or by an external stimulus (UV-light, magnetic field,…). The idea behind such a strategy is to play finely on the structure and/or interactions of the material at the nanometer scale to induce a large modification of the targeted macroscopic property to be controlled. Such an approach is especially suitable in the case of thin polymer films attached onto an interface in contact with a solution, owing to the possible applications in sensors, proteins repelling, adhesion, etc… The main question to answer when probing such systems is thus to describe the evolution of the conformation of the polymer thin layer as a function of the stimuli. To this aim, NR is then very powerful, simply because it enables to probe polymers at interfaces in solution on solid/liquid geometries with a good contrast, *e.g.* hydrogenated polymers in deuterated solvents. This is illustrated in Figure 13 representing the evolution on a cross-linked hydrogel of nanometric size of a thermo-sensible polymer (PNIPAM) tethered on a solid surface as function of temperature [27]. Such polymer has a Lower Critical Solubility Temperature in water T_{LCST} of 34°C, *i.e.* it collapses above T_{LCST}. Figure 13.b shows the evolution of the system as function of temperature. At low temperature, it shows damped fringes that are progressively more pronounced and shifted towards large q when increasing temperature. This qualitatively demonstrates that the system progressively collapses: the fringes amplitude increase owing to the increase of SLD' difference between the gel and the outside water due to progressive desolvation whereas the thickness reduces.

The volume fraction profiles extracted from the best fits confirm this qualitative approach (Figure 13.c). Below the LCST, the swelling of the gel depends on temperature and decreases when approaching T_{LCST}, whereas the gel is collapsed above T_{LCST}, even if expulsion of water is not complete ($\Phi(z=0)$ remains at 0.6 at 40°C). Please note that the mass of chains at the surface, that is the integral of the profile, is maintained at every concentration. Checking the mass conservation is indeed a good approach to constrain parameters during fitting.

4.4 Insight on specific part of a polymer chain: What is the distribution of chain ends in tethered chains?

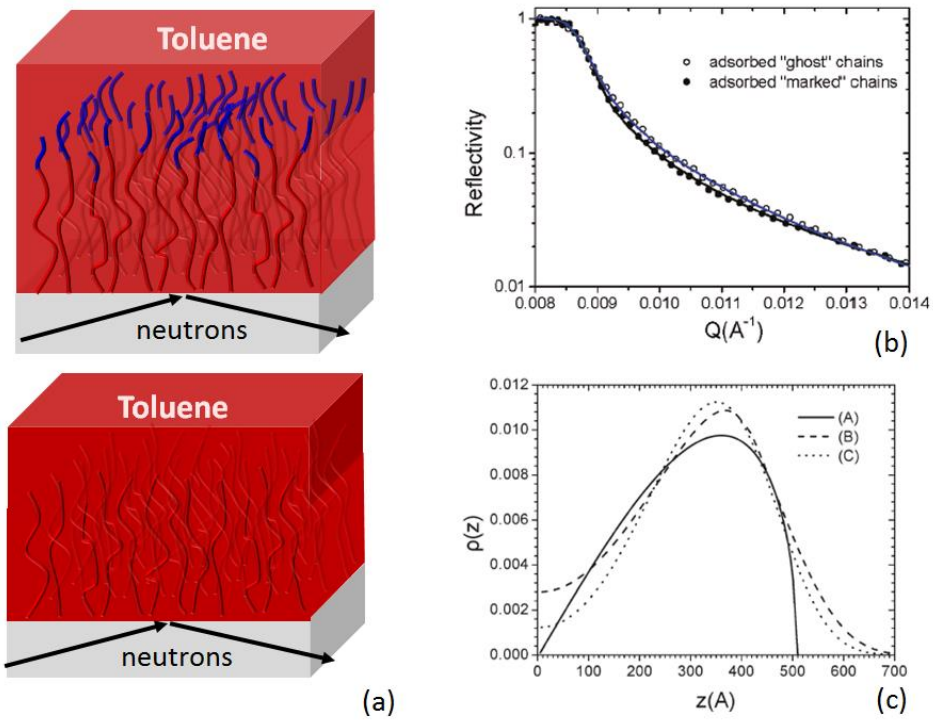

Figure 14: Distribution of chain ends in tethered brush from reference [28]. (a) Sketch of the system when the solvent (here toluene) has the same SLD as the deuterated PS chains in two situations: Measurement when the hydrogenated end chains are "marked" from the contrast points of view (top) and measurement with fully deuterated "ghost" chains. (b) Comparison of the experimental NR curves obtained respectively for ghost chains and marked chains. (c) Different profiles enabling to fit the NR data. Continuous line: Self-Consistent Theory; dashed line : modified analytical SCF theory; dotted line: Schulz function.

Contrast variation is also a powerful tool to probe some specific part of a polymeric chain. It has especially been used to measure the distribution of chain ends in tethered brushes in good solvent [28]. The principle is to achieve the synthesis of chains which are di-bloc polymers from the contrast point of view, namely chains for which the main part of the backbone is deuterated and the end is hydrogenated. A measurement in a solvent that matches the deuterated part of the chains allow then to probe only the hydrogenated chains ends, as shown in Figure 14.b that compares the NR curve measured in such contrast to those measured when the whole chains are deuterated and contrast-matched by solvent. Although the differences between these two NR curves are tiny, the determination of the specific contribution of the chain ends to the reflectivity is clearly achievable. The analysis of the experimental results was done both by simulation and by the Self-Consistent Theory. It supports the

picture that free ends are not localized at the brush height, but are distributed throughout the whole brush.

4.5 What is the interdigitation kinetics between a polymer melt and a polymer brush ?

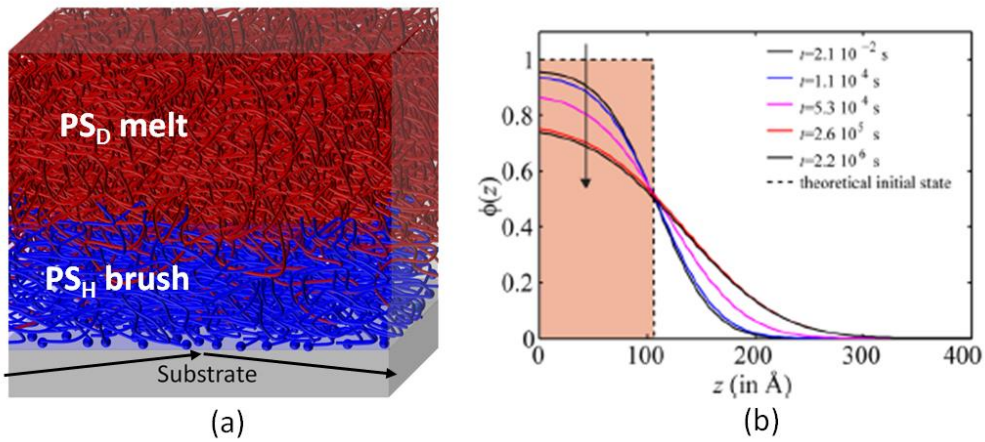

Figure 15: Probing the interdigitation kinetics between a polymer PS melt and a polymer PS brush [29]. (a) Sketch of the system from the contrast point of view; (b) Evolution of the segment density profile of the grafted chains for different annealing times for a given set of N_{brush}, σ and N_{melt}.

One of the case where NR is extremely powerful is for the study of interdiffusion processes between a thin polymer film in contact with a bulk polymer (brush/melt, melt/melt, brush/network, etc…). Indeed, this is the only one technique where it is possible to get some contrast between two melts of polymeric chains of the same chemical composition, provided that one is deuterated (see figure 15.a). The counterpart SANS experiment in bulk, *i.e.* the experimental verification of the Gaussian behavior of a chain within a melt, has been one of the milestone of neutron experiments for polymer science [30]. In NR, obviously only the interdiffusion SLD profile is probed but not the conformation. Since an NR measurement is an averaged static one, several measurements are then necessary to describe the kinetics. The strategy used is the following: The experimental system is let free to evolve at a given temperature above the T_g of the polymer for a given time t_1 outside the beam. It is then frozen below T_g and an NR measurement is done, which enables to capture a snapshot of the system at t_1. It is then possible to anneal the sample above T_g for a duration t_2 and to freeze the sample for a second measurement to capture the snapshot at t_2, and so on up to total equilibration of the system. Such an approach has been used in reference [29] to probe the kinetics of interdigitation of a PS brush in contact with a melt of the same homopolymer as function of the relevant molecular parameters of the system, namely the polymerization index of the chains from the brush N_{brush}, the grafting density of brushes σ and the polymerization index of the chains from the melt N_{melt}. This is illustrated in Figure 15.b that shows the segment density profile of the grafted chains for different annealing times for a given set of molecular parameters. It is then possible to extract a characteristic experimental time τ_{exp} from such series of profiles. The respective influences of N_{brush}, σ and N_{melt} on τ_{exp} can thus be finally probed in order to get a complete description of the interdigitation kinetics at the molecular level [29].

4.6 Ternary systems: behavior of a grafted brush in solution in presence of free chains

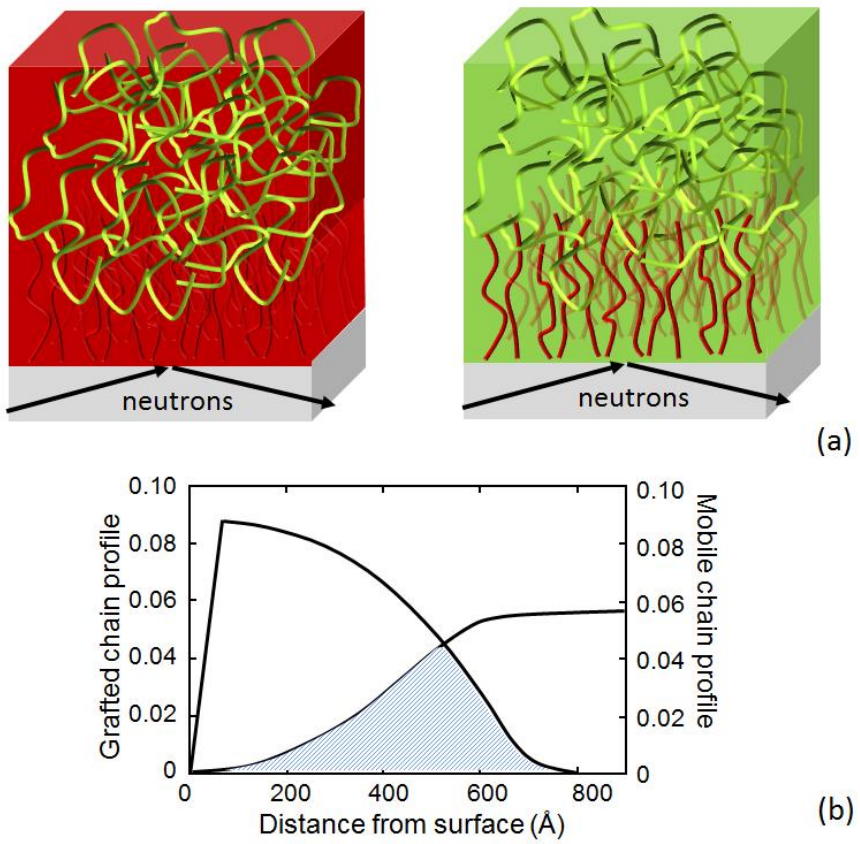

Figure 16: Contrast variation applied to the determination of the behavior of a grafted brush in solution in presence of free chains [31][32]. (a) Sketch of the system from the contrast point of view when the brush is contrast-matched by the solvent (left) or when the free chains are contrast-matched by the solvent (right); (b) Overview of the respective segment density profiles of the grafted chains and free chains, as obtained from the NR measurements in the contrast conditions depicted in (a).

The last example we present to depict the powerful possibilities of contrast variation is the case of a ternary system such as a mixture of two components in a solvent. In such a system, since the SLD of the solvent can be continuously tuned between those of the fully hydrogenated solvent and those of the fully deuterated one, it can be exactly adjusted to the SLD of one the component of the system, making it invisible to neutrons in order to probe specifically the structure of the other one, and *vice versa*. This strategy consisting in matching successively both components is routinely used in SANS but remains alas sparsely used in neutron reflectivity. This is illustrated for the case of the study of a tethered brush in a good solvent in contact with a semi-dilute solution of free chains of the same polymer species as the chains of the brush (Figure 16). In a first experiment, the SLD from the free chains was matched to determine the conformation of the chains of the brush. It appeared that the brush was contracted in presence of the free chains when $\Phi_{free} > \Phi_{brush}$, with respect to the case of the lone brush without free chains. This could either come from the equilibration of the osmotic pressure of the brush or from the penetration of the free chains within the brush that would screen the excluded-volume interactions [31]. In order to discriminate between these two hypotheses; it was mandatory to measure the SLD profile of the free chains in the vicinity of the surface by choosing a solvent matching the grafted chains. In such

a contrast, the measurements revealed a depletion layer close to the surface due to the presence of the "ghost" brush [32]. By plotting the density profiles corresponding to these two contrast (Figure 16.b), on can show that free chains penetrate strongly within the brush. Measurements with various grafting densities σ of the grafted brush revealed that free chains are progressively expelled from the brush upon increasing σ [32].

5 Conclusion

Since the pioneering works in the early 80's [33], Neutron reflectivity has become a mature and widespread technique that is rather easily accessible owing to the numerous reflectometers existing in all centers devoted to neutron scattering throughout the world. Due to its unique properties (isotopic labelling, study of buried interfaces), it is a unique and invaluable tool for the determination of structures at the nanometer scale in Soft Matter. In particular, despite of the expanding growth of microscopy techniques, it remains the only technique that gives *at the same time* the structure and composition from a liquid surface [16].

Acknowledgements

The authors warmly thank Max Wolff for his careful reading of the manuscript and his very useful remarks and suggestions.

References

[1] J. Penfold and R. K. Thomas, "The application of the specular reflection of neutrons to the study of surfaces and interfaces," *J. Phys. Condens. Matter*, vol. 2, no. 6, pp. 1369–1412, 1990.

[2] T. P. Russell, "X-ray and neutron reflectivity for the investigation of polymers," *Mater. Sci. Reports*, vol. 5, no. 4, pp. 171–271, 1990.

[3] H. P. Wacklin, "Neutron reflection from supported lipid membranes," *Curr. Opin. Colloid Interface Sci.*, vol. 15, no. 6, pp. 445–454, 2010.

[4] G. Fragneto-cusani, "Neutron reflectivity at the solid/liquid interface : examples of applications in biophysics," *J. Phys. Condens. Matter*, vol. 13, pp. 4973–4989, 2001.

[5] C. Fermon, F. Ott, and A. Menelle, "Neutron reflectivity," in *Daillant, J., Gibaud, A. (Eds.), X-ray and Neutron Reflectivity: Principles and Applications, Lect. Notes Phys. 770 (Springer, Berlin Heidelberg)*, 2009, pp. 183–234.

[6] M. Wolff, "Grazing incidence scattering," *EPJ Web Conf.*, 2018.

[7] V. Sears, "Neutron scattering lengths and cross sections," *Neutron news*, vol. 3, no. 3, pp. 26–37, 1992.

[8] "http://www.neutron.anl.gov/reference.html." .

[9] L. G. Parratt, "Surface Studies of Solids," *Phys. Rev.*, vol. 95, no. 2, 1954.

[10] S. A. Holt, P. Le Brun, C. F. Majkrzak, D. J. Mcgillivray, F. Heinrich, and L. Mathias, "An ion-channel-containing model membrane : structural determination by magnetic contrast neutron reflectometry," *Soft Matter*, vol. 5, pp. 2576–2586, 2009.

[11] R. A. Campbell, H. P. Wacklin, I. Sutton, R. Cubitt, and G. Fragneto, "FIGARO: The new horizontal neutron reflectometer at the ILL," *Eur. Phys. J. Plus*, vol. 126, no. 11, p. 107, 2011.

[12] F. Cousin, F. Ott, F. Gibert, and A. Menelle, "EROS II: A boosted time-of-flight reflectometer for multi-purposes applications at the Laboratoire Léon Brillouin," *Eur. Phys. J. Plus*, vol. 126, no. 11, p. 109, 2011.

[13] L. T. Lee, D. Langevin, and B. Farnoux, "Neutron Reflectivity of an Oil-Water Interface," *Phys. Rev. Lett.*, vol. 67, no. 19, pp. 2678–2681, 1991.

[14] J. Bowers, A. Zarbakhsh, J. R. P. Webster, L. R. Hutchings, and R. W. Richards, "Neutron Reflectivity Studies at Liquid - Liquid Interfaces : Methodology and Analysis," *Langmuir*, vol. 17, no. 1, pp. 140–145, 2001.

[15] L. Besnard, M. Protat, F. Malloggi, J. Daillant, F. Cousin, N. Pantoustier, P. Guenoun, and P. Perrin, "Breaking of the Bancroft rule for multiple emulsions stabilized by a single stimulable polymer," *Soft Matter*, vol. 10, no. 36, pp. 7073–7087, 2014.

[16] G. Fragneto and A. Menelle, "Progress in neutron reflectometry instrumentation," vol. 126, no. 11, p. 106, 2011.

[17] "http://www.ill.eu/." .

[18] "http://www-llb.cea.fr/." .

[19] "https://europeanspallationsource.se/section/ess-instrument-suite." .

[20] G. Fragneto, "Neutrons and model membranes," *Eur. Phys. J. Spec. Top.*, vol. 213, no. 1, pp. 327–342, 2012.

[21] R. L. T. Narayanan, H. Wacklin, O. Konovalov, "Recent applications of synchrotron radiation and neutrons in the study of soft matter," *Crystallogr. Rev.*, vol. 23, no. 3, pp. 160–226, 2017.

[22] L. Braun, M. Uhlig, R. Von Klitzing, and R. A. Campbell, "Polymers and surfactants at fluid interfaces studied with specular neutron reflectometry," *Adv. Colloid Interface Sci.*, vol. 247, pp. 130–148, 2017.

[23] O. Félix, Z. Zheng, F. Cousin, and G. Decher, "Are sprayed LbL-films stratified? A first assessment of the nanostructure of spray-assembled multilayers by neutron reflectometry," *Comptes Rendus Chim.*, vol. 12, no. 1–2, pp. 225–234, 2009.

[24] G. Decher, "Fuzzy Nanoassemblies: Toward Layered Polymeric Multicomposites," *Science (80-.).*, vol. 277, no. 5330, pp. 1232–1237, 1997.

[25] C. Devaux and J. Chapel, "Controlled structure and density of 'living' polystyrene brushes on flat silica surfaces," *Eur. Phys. J. E*, vol. 7, no. 4, pp. 345–352, 2002.

[26] C. Devaux, F. Cousin, E. Beyou, and J. P. Chapel, "Low swelling capacity of highly stretched polystyrene brushes," *Macromolecules*, vol. 38, no. 10, pp. 4296–4300, 2005.

[27] M. Li, B. Bresson, F. Cousin, C. Fretigny, and Y. Tran, "Submicrometric Films of Surface-Attached Polymer Network with Temperature-Responsive Properties," *Langmuir*, vol. 31, no. 42, pp. 11516–11524, 2015.

[28] N. Spiliopoulos, A. G. Koutsioubas, D. L. Anastassopoulos, A. A. Vradis, C. Toprakcioglu, A. Menelle, and G. Mountrichas, "Neutron Reflectivity Study of Free-End Distribution in Polymer Brushes," *Macromolecules*, vol. 42, no. 16, pp. 6209–6214, 2009.

[29] A. Chennevière, E. Drockenmuller, D. Damiron, F. Cousin, F. Boué, F. Restagno, and L. Léger, "Quantitative analysis of interdigitation kinetics between a polymer melt and a polymer brush," *Macromolecules*, vol. 46, no. 17, pp. 6955–6962, 2013.

[30] J. Cotton, D. Decker, H. Benoit, B. Farnoux, J. Higgins, G. Jannink, R. Ober, R. Picot, and J. des Cloizeaux, "Conformation of polymer chain in the bulk," *Macromolecules*, vol. 7(6), pp. 863–872, 1974.

[31] L. Lee, B. J. Factor, F. Rondelez, and M. S. Kent, "Structure of Tethered Polymer Chains Immersed in a Solution of Mobile Polymer," *Faraday Discuss.*, vol. 98, pp. 139–147, 1994.

[32] L. Lee and M. S. Kent, "Direct Measurement of the Penetration of Free Chains into a Tethered Chain Layer," *Phys. Rev. Lett.*, vol. 79, no. 15, pp. 2899–2902, 1997.

[33] J. B. Hayter, R. R. Highfield, B. J. Pullman, R. K. Thomas, A. I. McMullen, and J. Penfold, "Critical Reflection of Neutrons," *J. Chem. Soc., Faraday Trans. I*, vol. 77, pp. 1437–1448, 1981.

[34] Q. Berrod, K. Lagrené, J. Ollivier, and J.-M. Zanotti, "Inelastic and Quasi-Elastic Neutron Scattering. Application to Soft-Matter.," *EPJ Web Conf.*, 2018.